



On magnetophoretic separation of blood cells using Halbach array of magnets

Afshin Shiriny · Morteza Bayareh

Received: 3 March 2020 / Accepted: 2 August 2020 / Published online: 13 August 2020
© Springer Nature B.V. 2020

Abstract Magnetophoretic separation has gained much attention in recent years due to its easy application and low-cost fabrication compared to other active particle separation techniques. Due to the different properties of white blood cells (WBCs) and red blood cells (RBCs), it is possible to manipulate and separate them using a magnetic field. In this paper, a simple microfluidic device is proposed to fractionate WBCs and RBCs from whole blood using magnetophoretic force applied by Halbach array of three permanent magnets. Plasma streams containing WBCs and RBCs enter a simple microchip fabricated by PDMS. Permanent magnets apply positive and negative magnetophoretic forces to the RBCs and WBCs, respectively. Two cladding streams containing blood plasma are used to concentrate the cells in the magnetophoretic area. A wide range of inlet velocities and different distances of magnets from the channel (d) are investigated. It is demonstrated that the volume flow rate of core, and cladding streams, total flow rate and the distance between magnets and microchannel affect the separation efficiency individually. The results reveal that $d = 0.1, 0.2, 0.3, 0.4,$ and 0.5 mm may lead to complete separation when core and cladding flow rates are 1 and 7 $\mu\text{l/h}$, respectively.

Keywords Cell separation · Magnetophoresis · Microfluidic · Halbach array · RBCs · WBCs

1 Introduction

Microparticle separation is of great importance in the diagnostic, chemical, and biological analysis, as well as food processing and environmental assessment. The concept of separation can be generalized to genetic engineering, cellular transplantation, and immunology. Many investigations have been performed to improve microfluidic techniques to miniaturize the microfluidic devices. Particle separation based on microfluidic technology offers a simple, reliable, and cost-effective approach to disease detection. A microfluidic device can distinguish dead or cancerous cells from living and normal cells in the blood and separate them. Using unique micro-flow phenomenon features, various methods have been developed for continuous and accurate separation of microparticles. In general, particle separation is performed by two active and passive techniques. Passive methods use interactions between particles, microchannel structure, and fluid flow field to separate particles. These methods are easily measurable and do not depend on external forces, but their operating range is small due to their fixed geometry [1–3]. Common methods of passive separation include microfiltration [4–6], inertial separation [7–10], deterministic lateral

A. Shiriny · M. Bayareh (✉)
Department of Mechanical Engineering, Shahrekord
University, Shahrekord, Iran
e-mail: m.bayareh@sku.ac.ir

displacement (DLD) [11–14] and compact flow method [15–17]. Active methods are used to separate the particles using an external field such as electric, magnetic, optical, and acoustic fields. Active methods have more control over the separation processes and are more reliable. The separation efficiency of active methods is also greater than the passive ones. Active separation methods include dielectrophoresis [18–23], acoustophoresis [24–27] and magnetophoresis [28–63]. Magnetophoresis-based separation has received much attention in recent years due to its easier application and lower cost than other active separation methods [58]. For this reason, this technique is described in detail.

Magnetophoresis is a phenomenon in which the particle migrates in a magnetic field. This phenomenon can be divided into two general categories: positive and negative magnetophoresis. Positive magnetophoresis is the movement of a magnetic particle in a diamagnetic environment, and negative magnetophoresis is the migration of a diamagnetic particle in a magnetic environment. Magnetophoretic force is created when either the magnetic field gradient or the magnetization gradient of the environment, or a combination of both exist. This technique does not affect the properties of the sample solution, including pH, ion concentration, surface charge, and temperature. Besides, this method is easy to use and inexpensive. The key parameters for magnetophoretic applications are magnetic permeability (μ), magnetic flux density (B), and susceptibility (χ). The magnetic field is provided in the microfluidic devices using an electromagnet or permanent magnet. An electromagnet can produce a higher magnetic field gradient than a permanent one, which increases the separation efficiency. However, the permanent magnet is simpler to use and does not generate heat in the sample. An array of permanent magnets can be put together to increase the magnetic gradient. Magnetic susceptibility of particles and their surroundings is another important parameter in particle separation. Based on the susceptibility, the materials are divided into three categories: ferromagnetic ($\chi \gg 0$), paramagnetic ($\chi > 0$), and diamagnetic ($\chi < 0$). The magnetic susceptibility of the particles can be changed by their labeling using magnetic beads. Particle labeling increases the cost and time of the separation process. Negative magnetophoresis is a method without labeling to separate diamagnetic particles such as cells in a paramagnetic

medium, for example, ferrous solutions. The diamagnetic particles in the ferrofluids act as magnetic holes. If the system is exposed to an external magnetic field, the imbalance of the particle and fluid susceptibility creates a negative magnetophoretic force, leading to that the particles move away from the magnet. The negative magnetophoretic force is also proportional to the particle size so that the particles can be separated due to their size [45, 55, 57]. Negative magnetophoresis has attracted considerable attention in recent years in the fields of disease diagnosis, therapeutic studies, concentration, and cell fractionation [58].

Pamme and Mans [29] proposed a free-flow magnetophoresis for continuous flow separation of magnetic particles. In this method, the sample enters the channel and is driven by a cladding flow toward the channel wall. Then, a magnetic field perpendicular to the direction of fluid flow is applied to the magnetic particles. Non-magnetic particles move directly to the channel outlet, while magnetic ones move transverse and are separated based on their size and magnetization. Adams et al. [34] developed a method for particle separation using multi-target magnetic cell separator. They separated magnetic particles with an output power of 10^9 cells per hour and reached a purity of about 90%. Mizuno et al. [41] used a combination of hydrodynamic filtration and magnetophoresis to separate lymphocyte cells. In this method, the cells are first divided into two groups by a size-based hydrodynamic filter, and then each group is separated due to their magnetic labels. Nam et al. [42] used a magnetic field to separate malaria-infected red blood cells and achieved 98.3% separation efficiency. Zhu et al. [43] used a combination of positive and negative magnetophoretic forces to separate the magnetic particles from non-magnet ones and particles with different magnetizations. Zhang et al. [49] proposed a microfluidic device based on negative magnetophoresis to separate 4- and 13- μm polystyrene particles using a 4-mm neodymium magnet at a distance of 1 mm from the channel. Hejazian and Nguyen [47] experimentally separated non-magnet polystyrene particles of sizes 3.1 and 4.8 μm suspended in a paramagnetic solution flowing through a straight microchannel of 1 mm width and 500 μm height. They employed an array of permanent magnets on either side of the channel. Tarn et al. [52] separated 5- and 10- μm diamagnetic particles based on their size and magnetization in a paramagnetic solution. They reported that the

deviation of particles concerning the channel center increases along the microchannel by increasing their size and magnetization. Munaz et al. [58] designed a negative magnetophoresis-based microfluidic device for the separation of fluorescent polystyrene microparticles with diameters of 3.2 and 4.8 μm using two different geometries using two-stream and three-stream structures. Experimental results showed that the highest separation efficiency corresponds to the three-stream structure. It was 78% and 75% for the 3.2- and 4.8- μm particles, respectively. Wu et al. [60] investigated a microfluidic device based on negative magnetophoresis for separating of 5- and 12- μm fluorescent polystyrene particles experimentally and numerically. They concluded that the Halbach array results in better performance than the other configuration. They also reported that the deflection angle increases with flow rate, magnetic field, and particle size.

Magnetic separation of blood cells using microfluidic devices has been previously reported [28, 30–33, 36, 37, 39, 62, 63]. Due to the different properties of WBCs and RBCs, it is possible to manipulate and separate them using a magnetic field [39]. Han and Frazier [30, 31] modeled a magnetophoretic separator to separate WBCs and RBCs based on their intrinsic magnetic properties. Furlani [33] proposed a continuous and label-free method for separating of WBCs and RBCs in plasma using magnetic force. Seo et al. [36, 37] used a combination of hydrodynamic forces and magnetophoresis to increase the output power of blood cell separation. Their experimental results showed that separation efficiency depends on the magnetophoretic force.

In the present paper, the separation of WBCs and RBCs from whole blood is simulated numerically using a magnetophoretic force using Halbach array of three permanent magnets. Two cladding flows are used to concentrate the particles in the area under the magnetic field. To the best of our knowledge, the separation of bold cells has not been carried out using Halbach arrays of magnets. On the other hand, the proposed microdevice can be easily fabricated, and its separation efficiency reaches 100% for a relatively wide range of throughputs. The numerical results are analyzed by changing the magnet array distance from the channel and the ratio of inlet streams.

2 Governing equations

Figure 1 shows a schematic of the microfluidic device. WBCs and RBCs suspended in the blood plasma enter the microfluidic device and are separated by a magnetophoretic mechanism. The main microchannel has a rectangular cross-section with the length of $L = 20\text{ mm}$, the width of $W = 200\ \mu\text{m}$, and depth of $H = 20\ \mu\text{m}$. Whole blood containing plasma and WBCs and RBCs is injected into the microfluidic chip using a syringe pump with $Q = 5\ \mu\text{L/h}$. Two cladding flows containing plasma without WBCs and RBCs are injected into other entrance channels to concentrate blood cells in the central area of the main channel. The described symmetric microchannel can be easily fabricated using Polydimethylsiloxane (PDMS) [67]. To produce a non-uniform magnetic field, an array of three NdFeB permanent magnets with dimensions of $5 \times 5 \times 5\ \text{mm}^3$ is placed in the distance d from the microchannel wall, as shown in Fig. 2. In this study, the magnets are positioned alongside the microchannel in the Halbach array. This arrangement strengthens the magnetic field on one side of the magnet [60].

The magnetophoretic separation of cells is a combination of electromagnetic, fluidic, and particle dynamics [39]. To solve the magnetic field statically (magnetostatic equations), the Maxwell-Ampere’s law is employed for the magnetic field [44, 49, 58, 64]:

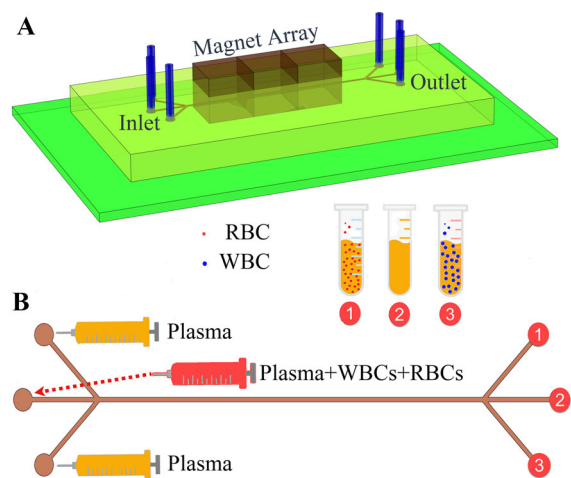


Fig. 1 Magnetophoretic separation of WBCs and RBCs within blood plasma: **a** Schematic of the microfluidic device, and **b** structure of microchip along with its inlets and outlets

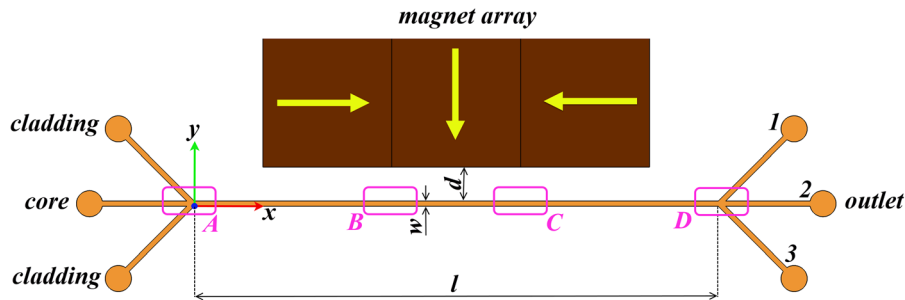


Fig. 2 Geometrical parameters of the problem (yellow arrows indicate the direction of magnetization)

$$\vec{H} = -\nabla V_m \tag{1}$$

where H is the magnetic field strength, and V_m is scalar magnetic potential. Using Gauss’s law for magnetic flux density B , the following equation is concluded [44, 49, 58, 64]:

$$\nabla \cdot \vec{B} = 0 \tag{2}$$

The relationship between B and H in the fluid and in the magnet domain is shown in Eqs. 3 and 4, respectively [44, 49, 58, 64]:

$$\vec{B} = \mu_0 \mu_r \vec{H} \tag{3}$$

$$\vec{B} = \mu_0 (\vec{H} + \vec{M}) \tag{4}$$

where $\mu_0 = 4\pi \times 10^{-7}$ (T m/A) (T m/A) is the air permeability coefficient, μ_r is the relative magnetic permeability of the fluid or environment, and M (A/m) is the magnetization of the magnet. It should be noted that the relative magnetic permeability can be calculated as follows [44, 49, 58, 64]:

$$\mu_r = 1 + \chi \tag{5}$$

The governing equations of the fluid flow are the continuum and Navier–Stokes equations:

$$\nabla \cdot \vec{u}_f = 0 \tag{6}$$

$$\rho_f \vec{u}_f \cdot \nabla \vec{u}_f = -\nabla p + \mu_f \nabla^2 \vec{u}_f \tag{7}$$

where u_f is the fluid velocity (blood plasma), μ_f is the dynamic viscosity, ρ_f is the fluid density, and p is the fluid pressure. Plasma is considered to be incompressible Newtonian fluid. The properties used for plasma and blood cells are presented in Table 1.

Since the density of cells is close to the cladding solution (the blood plasma), the dominant force

governing the particles is the hydrodynamic drag force (F_D) [29, 55] and magnetophoretic force (F_M). The particle trajectory is described using Newton’s second law:

$$m_p (d\vec{u}_p/dt) = \vec{F}_D + \vec{F}_M \tag{8}$$

where m_p is the particle mass and u_p is its velocity. Since the flow rate in microfluidic devices is very low, the flow is assumed to be laminar. The Reynolds number for the present work is $Re = 0.05$, which confirms that the flow regime is laminar.

$$Re = \rho_f U_{in} D_h / \mu_f \tag{9}$$

where $U_{in} = Q/WH$ is inlet velocity and D_h is hydraulic diameter defined as follows:

$$D_h = 2WH/(W + H) \tag{10}$$

Hydrodynamic drag force is calculated using Stokes’ law by assuming blood cells as spherical microparticles for low Reynolds numbers [33, 35]:

$$\vec{F}_D = 3\pi d_p \mu (\vec{u}_f - \vec{u}_p) \tag{11}$$

The magnetophoretic force is calculated using Eq. 12 [35, 45, 52] by neglecting the magnetoviscosity effects for microparticle concentrations less than 1% [65]:

$$\vec{F}_M = \frac{V_p}{\mu_0} (\chi_p - \chi_f) (\vec{B} \cdot \nabla) \vec{B} \tag{12}$$

where $V_p = \frac{1}{6} \pi d_p^3$ is the volume of the particle. By placing Eqs. 3 and 5 in Eq. 12, the magnetophoretic force is [49, 58]:

$$\vec{F}_M = 2\pi r_p^3 \mu_0 \mu_{r,f} K \nabla \vec{H}^2 \tag{13}$$

Table 1 Physical properties of blood contents [33, 62, 63]

	ρ (kg/m ³)	ρ (kg/m ³)	μ (Pa s)	X	d_p (μ m)
Plasma	1000	1000	0.001	-7.7×10^{-6}	–
WBCs	1070	1070	–	-9.9×10^{-6}	10
RBCs	1100	1100	–	-3.9×10^{-6}	7

$$K = \frac{\mu_{r,p} - \mu_{r,f}}{\mu_{r,p} + 2\mu_{r,f}} \tag{14}$$

where r_p is the radius of the particle. $\mu_{r,f}$, and $\mu_{r,p}$ are the relative magnetic permeability of the fluid and the particle, respectively. Since the direction of the magnetic field is perpendicular to the direction of the fluid flow in microfluidic devices, the particle velocity u_p can be obtained by equating drag and magnetophoretic forces under equilibrium position [45, 52]:

$$\vec{F}_D + \vec{F}_M = 0 \tag{15}$$

By placing the definition of \vec{F}_D from Eq. 11 in Eq. 15,

$$3\pi d_p \mu (\vec{u}_f - \vec{u}_p) + F_M = 0, \tag{16}$$

the particle velocity can be calculated as follows:

$$\vec{u}_p = \vec{u}_f + (\vec{F}_M / 3\pi d_p \mu_f) \tag{17}$$

The rate of cell collection or cell separation efficiency can also be calculated using Eq. 16 [36, 39, 58]:

$$SE(\%) = \frac{N_O}{N_T} \times 100 \tag{18}$$

where N_O and N_T are numbers of cells passing through the outlet and the total number of cells entering the microchannel, respectively.

The governing equations are solved by the finite element method using COMSOL Multiphysics 5.5 software. The relative magnetic permeability of the space around the microchannel and the magnets is set to one, and the magnetization of the magnets is $M = 9.9 \times 10^5$ A/m [60]. No-slip boundary condition is imposed on the microchannel walls, and constant pressure condition is used for the output. WBCs and RBCs enter the microchannel at an initial velocity equal to the fluid velocity through the central inlet channel.

3 Validation

To validate the numerical method, the results of the present simulation are compared with those of He et al. [66], who investigated the effect of magnetic manipulation on label-free nonmagnetic particles (Figs. 3 and 4). Figure 3 shows the magnetic field’s strength in terms of channel length along the centreline of a straight microchannel containing diamagnetic microparticles within a magnetic fluid exposed to a non-uniform magnetic field generated by a permanent magnet. Figure 4 presents the corresponding magnetic force. The distribution of negative magnetophoretic force along and perpendicular to the fluid stream, i.e., F_{mx} and F_{my} , respectively, is compared with the reference results, indicating very good agreement.

For more verification, the separation of diamagnetic microparticles suspended in a conventional ferrofluid with poly ethylene oxide (PEO) flowing in a straight microchannel exposed to a permanent magnet is compared with numerical and experimental results of Zhang et al. [49]. The ratio of lateral velocity to the horizontal velocity of microparticles along the microchannel is shown in Fig. 5 for different inlet flow rates. It should be pointed out that the PEO-based

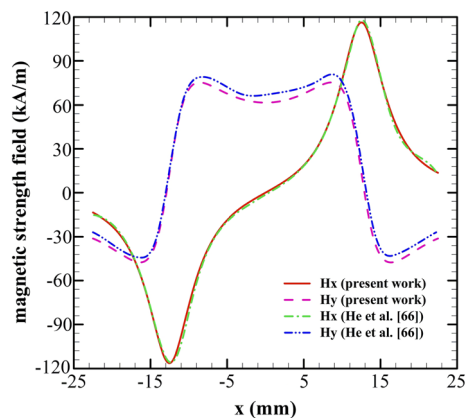


Fig. 3 Magnetic field strength along the channel centerline

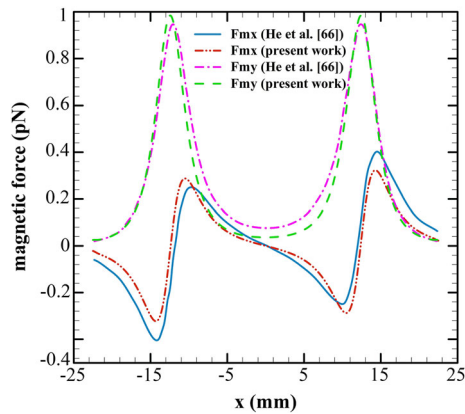


Fig. 4 Magnetophoretic force along the channel centerline

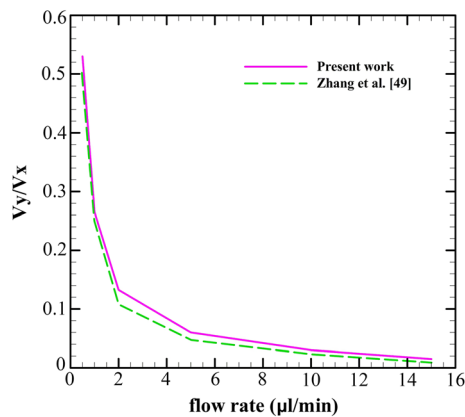


Fig. 5 The ratio of lateral velocity to horizontal velocity of microparticles along the microchannel

ferrofluid exhibits viscoelastic behavior. However, as Zhang et al. [49] reported, the effect of elastic force can be neglected in the present simulations due to the low channel aspect ratio. Besides, in Fig. 6, the separation of 5- and 13- μm magnetic particles within the PEO-based ferrofluid is compared with the numerical results of Zhang et al. [49]. They carried out the numerical modeling of magnetophoretic separation of microbeads using COMSOL Multiphysics 5.1. In this figure, the colored contours show the distribution of the magnetic field strength. It is demonstrated that larger microbeads are repelled more quickly toward the opposite wall compared to the smaller ones. As can be seen, there is a very good agreement between the present results and those of Zhang et al. [49].

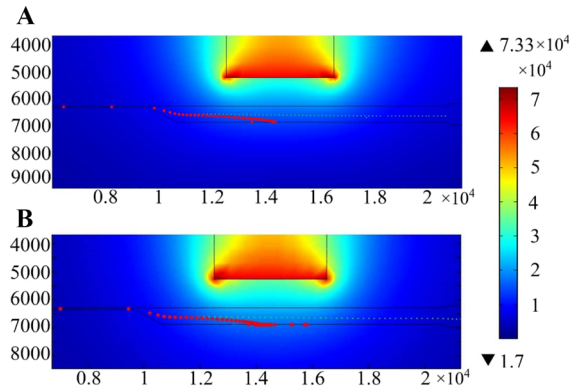


Fig. 6 Numerical simulation of magnetophoretic separation of 5- and 13- μm microparticles suspended in the PEO-based ferrofluid (color contour indicates the magnetic field strength, A/m): **a** present work, and **b** the results of Zhang et al. [49]

4 Grid study

The structured grid is used for the microchannels, and a triangular one is employed for the surrounding space (Fig. 7). The average magnetic field strength along the microchannel centerline, lateral velocity, and lateral position of the WBCs at the output of the main channel are presented in Table 2 for the grids with 25,000, 90,000, 200,000, and 350,000 elements. The results demonstrate that the grid resolution of 200,000 can be selected for further simulations.

5 Results

The distribution of the magnetic field for the magnet with the distance of $d = 1$ mm to the microchannel is shown in Fig. 8. In this figure, three magnets with a Halbach arrangement are positioned at different distances from the microchannel wall. This arrangement extends the magnetic field from one side to the farther distances. The red lines represent the distribution of the induced magnetic field. In the Halbach array of magnets, the magnets' polarization angles rotate as much as 90° . The yellow arrows show the direction of the magnetization.

In Fig. 9, the distribution of the magnetic field density along the microchannel centreline is plotted for different distances of the magnet array from the channel. As can be seen, the magnitude of the magnetic field decreases by increasing the distance from the microchannel. The magnetic field peak points

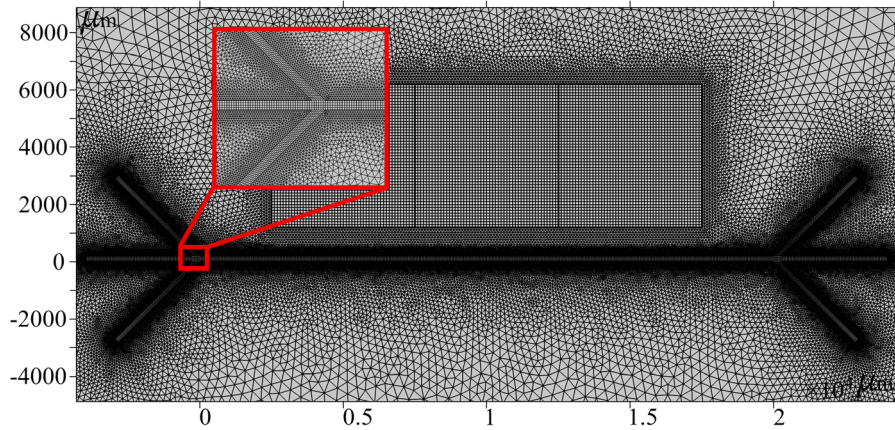


Fig. 7 The grid used for present simulations

Table 2 The results of the grid study

Number of elements	Averaged magnetic strength field along the centerline $H \times 10^5$ (A/m)	Lateral velocity of RBCs in the outlet ($\mu\text{m/s}$)	Lateral position of RBCs in the outlet (μm)
25,000	4.5196	21	153
90,000	4.5196	45	147
200,000	4.5196	45	146
325,000	4.5196	46	146

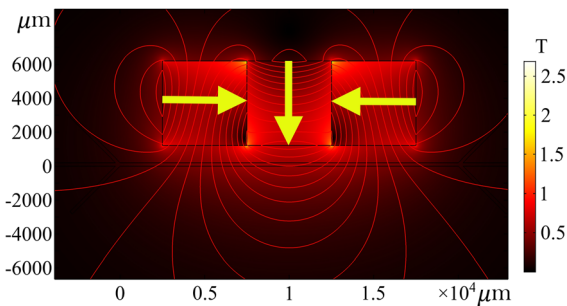


Fig. 8 The density distribution of the magnetic field where the magnet array has a distance of $d = 1$ mm from the microchannel. The red lines represent the induced magnetic field, and the yellow arrows indicate the direction of the magnetization

are created where the induced magnetic field of central magnet reaches those of side magnets. As the magnet array distance from the microchannel decreases, the value of these peak points becomes larger.

A strong magnetic field is required to separate these cells due to the slight difference in the relative magnetic permeability coefficient of plasma and blood cells. Thus, the distance between the array of magnets

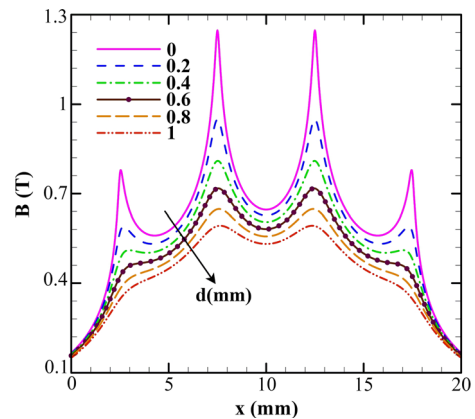


Fig. 9 Magnetic field density $B(T)$ along the microchannel centreline for different distances of magnet array from the microchannel (d)

and main channel is assumed to be $0 \leq d \leq 1$ (mm). The relative permeability coefficient of RBCs is greater than that of plasma. Hence, a positive magnetophoretic force is exerted on RBCs under a non-uniform magnetic field, leading to their migration toward higher magnetization region, i.e. magnets. For

the case of WBCs, a negative magnetophoretic force pushes them toward the farther microchannel outlet due to their lower relative magnetic permeability coefficient than plasma. Figure 10 presents the vertical and horizontal components of the magnetophoretic force applied to the RBCs and WBCs along the centreline of the microchannel for different values of d . As the magnet distance from the microchannel increases, the magnetophoretic force decreases. It is demonstrated that the vertical component of the magnetic force applied to WBCs is higher than that exerted on RBCs. For example, $|F_{my}|$ is 0.154 and 0.25 pN for RBCs and WBCs, respectively, for $x = 7.51$ mm and $d = 0.6$ mm.

In order to concentrate suspending blood cells in the main microchannel that is under the influence of magnetophoretic force (to increase the separation efficiency), two cladding streams containing only blood plasma enters through two inlets (Fig. 2). Another important factor affecting the separation of particles is the inlet flow rate. The high inlet velocity

leads to that the hydrodynamic force (the drag Stokes force) overcomes the magnetophoretic force, resulting in a reduction in the separation efficiency. On the other hand, very low velocity of the fluid containing particles causes the magnetophoretic force to overcome the drag force, leading to that the particles are trapped within the main channel and accumulated in the vicinity of the channel walls. In addition, the ratio of the cladding flow rate to the core flow rate may cause the particle to be concentrated in the centreline of the main channel. Therefore, the optimal value of this ratio is a key factor of particle separation effectively. In this paper, a wide range of different ratios of cladding flow and inlet core flow is investigated. In general, total flow rates of 7.5, 15, and 30 $\mu\text{L}/\text{h}$ are considered. Figure 11 shows an example of a complete separation of RBCs and WBCs for $d = 0.2$ mm and a total flow rate of $Q = 15$ $\mu\text{L}/\text{h}$. The time-dependent Eulerian approach is used to trace particles. The convergence criterion is set to 10^{-5} and the time step is 1 ms. Steady fluid flow in the

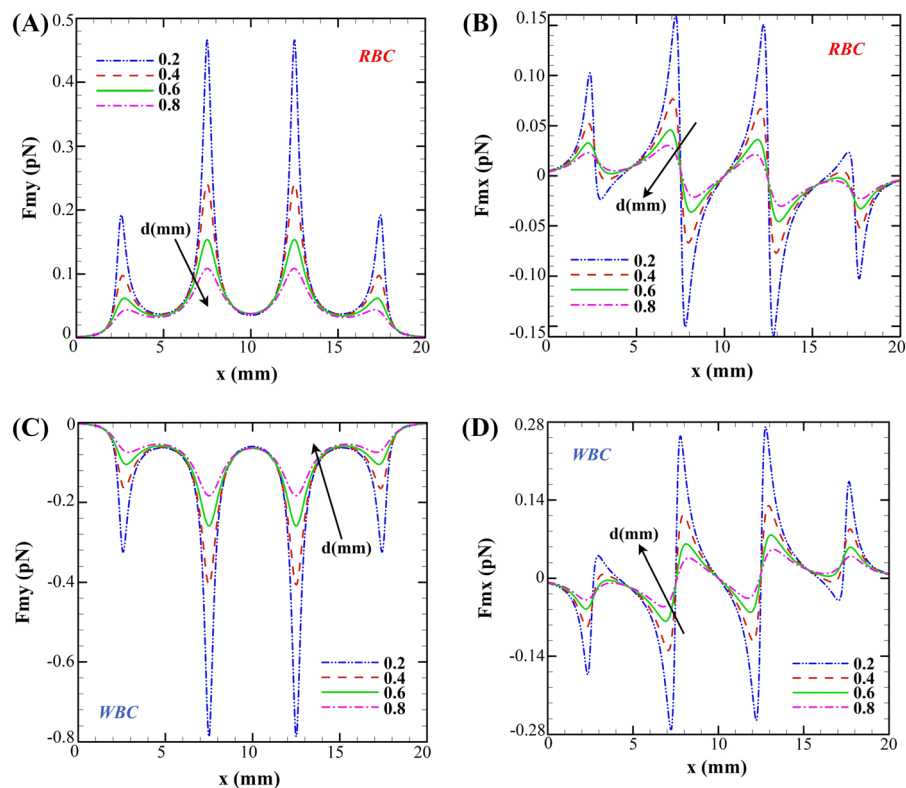


Fig. 10 a, c The vertical, and b, d horizontal components of the magnetophoretic force applied to the RBCs and WBCs along the centreline of the microchannel for different values of d

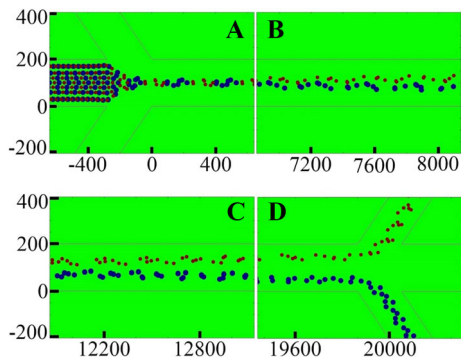


Fig. 11 Particle trajectories and separation of WBCs (blue) and RBCs (red) for core flow rate of 3 $\mu\text{L/h}$, cladding flow rate of 6 $\mu\text{L/h}$ and $d = 0.2$ mm

microchannel is solved in the absence of blood cells. Figure 12 shows velocity contours throughout the microchannel for core flow rate of 3 $\mu\text{L/h}$, cladding flow rate of 6 $\mu\text{L/h}$ and $d = 0.2$ mm and demonstrates that the fluid flow becomes fully developed along the channel. As indicated in this figure, the parabolic velocity profile is formed at all channel cross sections. The maximum velocity remains constant with the channel length. The obtained velocity field solution is used when the particles enter the channel. Seven RBCs and seven WBCs are injected into the microchannel at each time step. Section A shows the main microchannel inlet. As can be seen, the particle focusing is generated in the vicinity of the channel centerline for exposure to the magnetic field. The highest cell separation rate occurs in sections B and C with the magnetization of 0.375 W and 0.625 W, respectively.

For cladding and core flow rates of 6 and 3 $\mu\text{L/h}$, respectively, and $d = 0.2$ mm, the complete separation of RBCs and WBCs can be achieved.

Particle trajectories of blood cells in the main channel is plotted in Fig. 13 for two volume flow rates of 7.5 and 15 $\mu\text{L/h}$ and $d = 0.2$ mm. Three different values of cladding and core flow rates are considered as follows: (cladding flow rate, core flow rate, cladding flow rate) = (2.5, 2.5, 2.5), (3, 1.5, 3), and (3.5, 0.5, 3.5) for $Q = 7.5$ $\mu\text{L/h}$ and (5, 5, 5), (6, 3, 6), (7, 1, 7) for $Q = 15$ $\mu\text{L/h}$. As the cladding flow rate increases relative to the core flow, particle motion becomes more concentrated, but the magnetophoretic force overcomes the hydrodynamic drag force causing more deviation of the cells from the microchannel walls due to the deceleration of the particles. In this case, it is possible to trap the cells in the channel. In other words, the blood cells can be directed to the outlet by increasing the distance between the magnets and the microchannel (reducing the magnetophoretic force).

Figure 14 shows the particle trajectories of blood cells for volume flow rates of (3.5, 0.5, 3.5) and (7, 1, 7) $\mu\text{L/h}$ and different values of d . This figure confirms that, for $Q = 7.5$ $\mu\text{L/h}$, the particle separation is performed better as the magnetic force decreases. It is shown that the best performance of the chip for the volume flow rate of 7.5 $\mu\text{L/h}$ is achieved when $d = 0.8$ and 1 mm. For $Q = 15$ $\mu\text{L/h}$, as the distance between the magnets and microchannel decreases, the particle deviation from the channel centreline increases. It can be observed that $d = 0.2, 0.4,$ and 0.6 mm may result in more appropriate positions of magnet array. It can be concluded that the

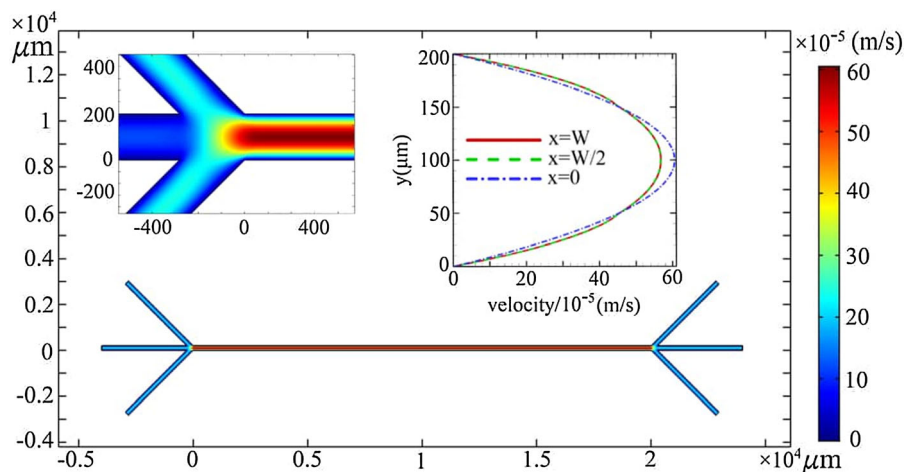


Fig. 12 Velocity contour throughout the microchannel for core flow rate of 3 $\mu\text{L/h}$, cladding flow rate of 6 $\mu\text{L/h}$ and $d = 0.2$ mm

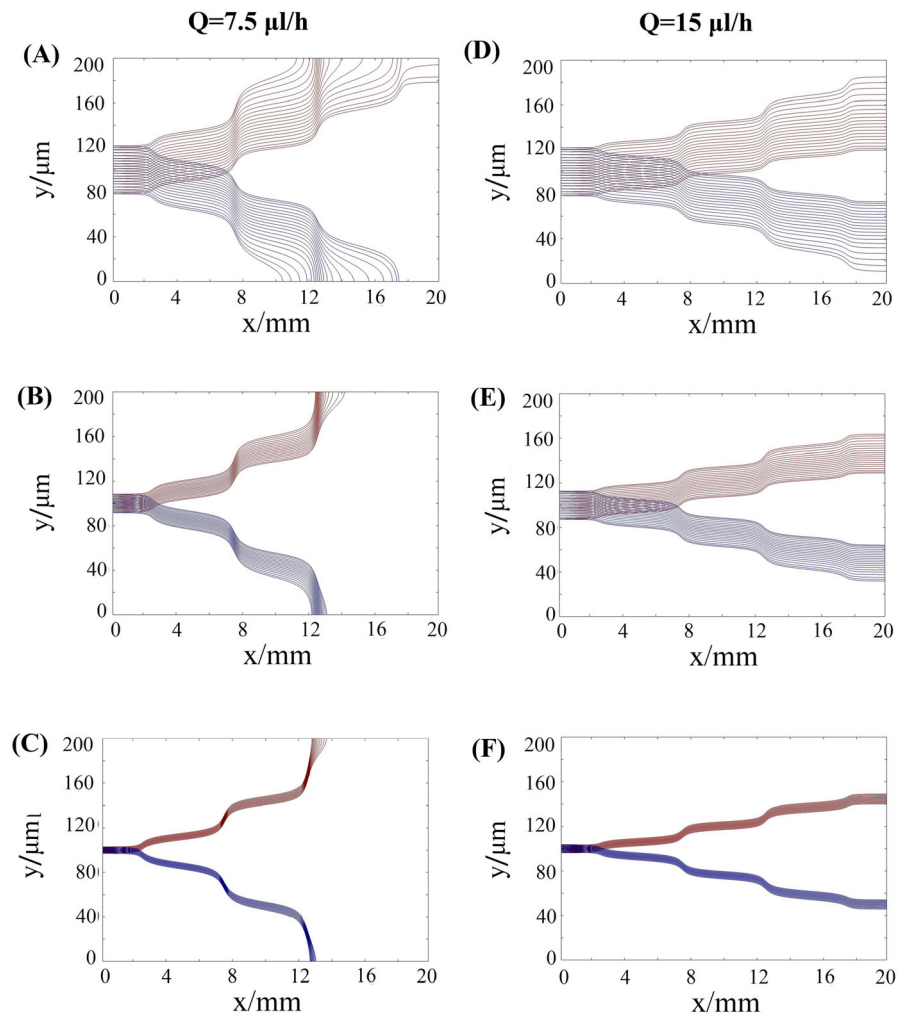


Fig. 13 Particle trajectories of blood cells for $d = 0.2$ mm and: (cladding flow rate $\mu\text{l/h}$, core flow rate $\mu\text{l/h}$, cladding flow rate $\mu\text{l/h}$) = **a** (2.5, 2.5, 2.5), **b** (3, 1.5, 3), **c** (3.5, 0.5, 3.5), **d** (5, 5, 5), **e** (6, 3, 6), **f** (7, 1, 7)

volume flow rate of core and cladding channels, total flow rate, and the distance between magnets and microchannel affect the separation efficiency individually. In other words, there are optimal conditions in which the separation efficiency becomes 100% according to different magnitudes of these parameters.

Figure 15 shows separation efficiency for different values of d and various volume flow rates of cladding and core channels. This figure demonstrates that the volume flow rates of (3.5, 0.5, 3.5) is more efficient for $Q = 7.5$ $\mu\text{l/h}$, where separation efficiency is 100% for $d = 0.8, 0.9$, and 1 mm. For the case of (3, 1.5, 3), $d = 0.9$ and 1 mm results in $SE = 100\%$, and complete

separation does not occur when the volume flow rates are (2.5, 2.5, 2.5). Different results are obtained for the case of $Q = 7.5$ $\mu\text{l/h}$. While $SE = 100\%$ does not occur for volume flow rates of (5, 5, 5), there are several magnet array positions, i.e., $d = 0.1, 0.2, 0.3, 0.4$ and 0.5 mm, in which complete particle separation happens when core and cladding flow rates are (7, 1, 7).

6 Conclusions

In this work, a simple microfluidic device was proposed to fractionate WBCs and RBCs from whole

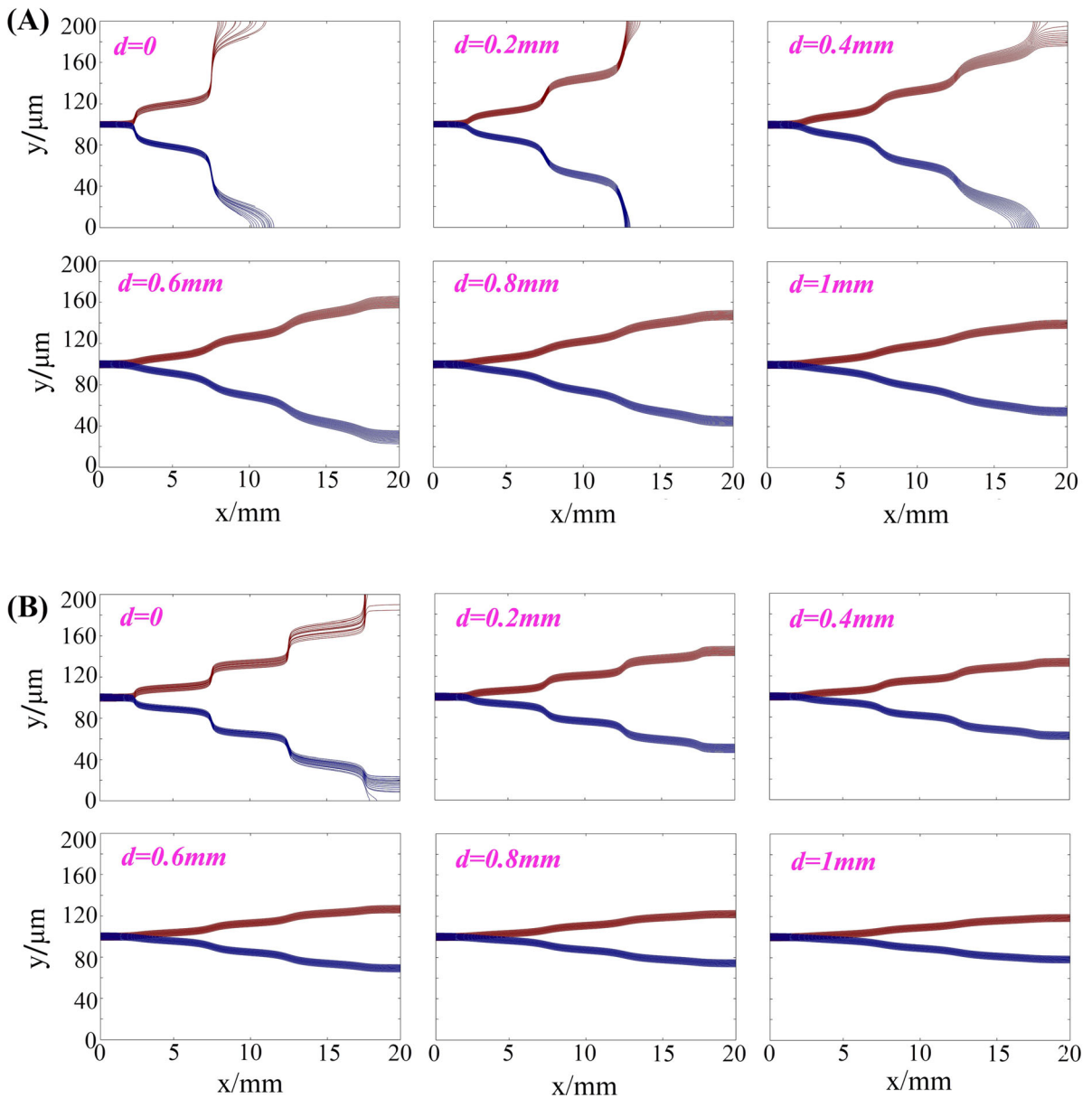


Fig. 14 Particle trajectories of blood cells for (cladding flow rate $\mu\text{l/h}$, core flow rate $\mu\text{l/h}$, cladding flow rate $\mu\text{l/h}$) **a** (3.5, 0.5, 3.5), **b** (7, 1, 7) and different values of d

blood using a Halbach array of three permanent magnets. In order to concentrate the particles, two cladding flows were used. The numerical results were analyzed by changing the magnet array distance from the channel and the ratio of core and cladding streams. Total flow rates of 7.5 $\mu\text{l/h}$ and 15 $\mu\text{l/h}$ were considered to evaluate the influence of the relative flow rate of cladding streams. In addition, different distances between the Halbach array of magnets and main

channel were examined. The results demonstrated that the volume flow rate of core and cladding channels, total flow rate and the distance between magnets and microchannel affect the separation efficiency individually. It was revealed that the volume flow rates of (3.5, 0.5, 3.5) is more efficient for $Q = 7.5 \mu\text{l/h}$, where separation efficiency is 100% for $d = 0.8, 0.9,$ and 1 mm. the results showed that complete particle

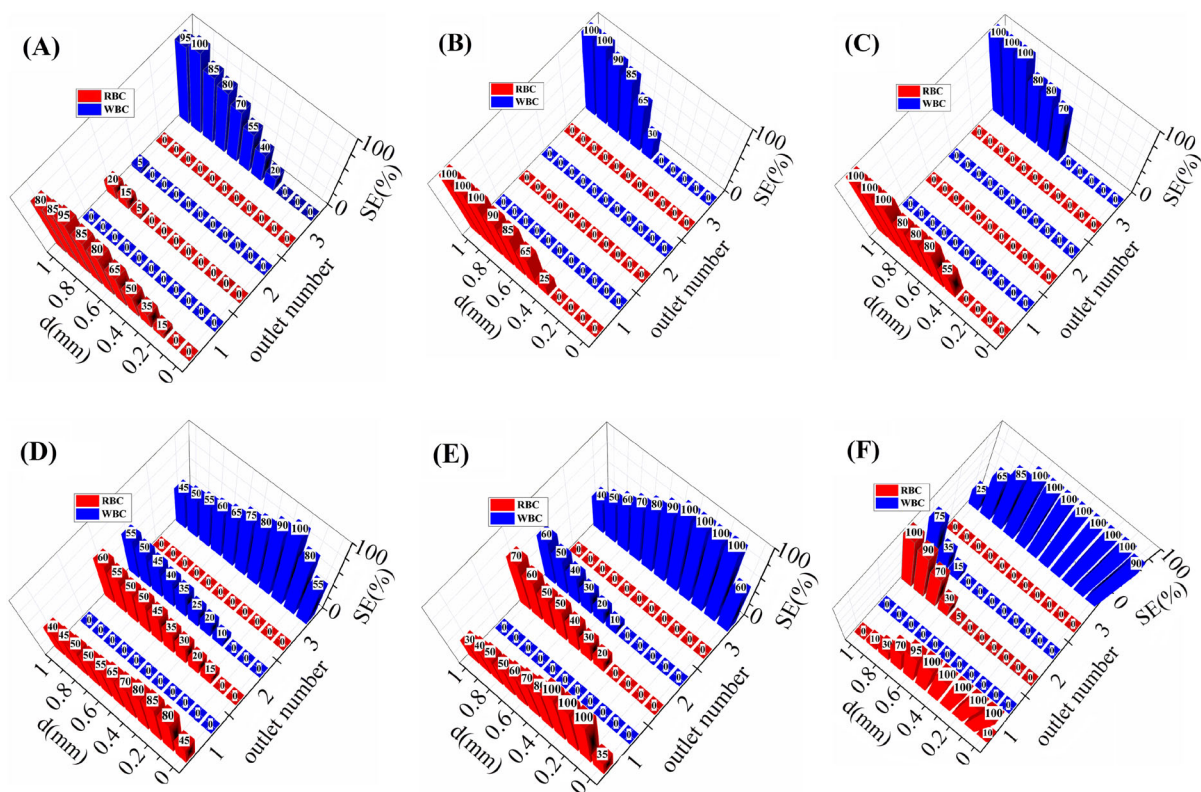


Fig. 15 Separation efficiency for (cladding flow rate $\mu\text{l/h}$, core flow rate $\mu\text{l/h}$, cladding flow rate $\mu\text{l/h}$) = **a** (2.5, 2.5, 2.5), **b** (3, 1.5, 3), **c** (3.5, 0.5, 3.5), **d** (5, 5, 5), **e** (6, 3, 6), **f** (7, 1, 7), and different values of d

separation happens when core and cladding flow rates are (7, 1, 7) and $d = 0.1, 0.2, 0.3, 0.4$ and 0.5 mm.

Compliance with ethical standards

Conflict of interest The authors declare that they have no conflict of interest.

References

- Dalili A, Samiei E, Hoorfar M (2019) A review of sorting, separation and isolation of cells and microbeads for biomedical applications: microfluidic approaches. *Analyst* 144(1):87–113
- Sajeesh P, Sen AK (2014) Particle separation and sorting in microfluidic devices: a review. *Microfluid Nanofluid* 17(1):1–52
- Yan S, Tan SH, Li Y, Tang S, Teo AJ, Zhang J, Zhao Q, Yuan D, Sluyter R, Nguyen N-T (2018) A portable, hand-powered microfluidic device for sorting of biological particles. *Microfluid Nanofluid* 22(1):8
- Chen J, Chen D, Yuan T, Chen X, Xie Y, Fu H, Cui D, Fan X, Oo MKK (2014) Blood plasma separation microfluidic chip with gradual filtration. *Microelectron Eng* 128:36–41
- Kang Y-T, Doh I, Byun J, Chang HJ, Cho Y-H (2017) Label-free rapid viable enrichment of circulating tumor cell by photosensitive polymer-based microfilter device. *Theranostics* 7(13):3179
- Liu C, Mauk M, Gross R, Bushman FD, Edelstein PH, Collman RG, Bau HH (2013) Membrane-based, sedimentation-assisted plasma separator for point-of-care applications. *Anal Chem* 85(21):10463–10470
- Amini H, Lee W, Di Carlo D (2014) Inertial microfluidic physics. *Lab Chip* 14(15):2739–2761
- Di Carlo D, Irimia D, Tompkins RG, Toner M (2007) Continuous inertial focusing, ordering, and separation of particles in microchannels. *Proc Natl Acad Sci* 104(48):18892–18897
- Martel JM, Toner M (2012) Inertial focusing dynamics in spiral microchannels. *Phys Fluids* 24(3):032001
- Rafeie M, Zhang J, Asadnia M, Li W, Warkiani ME (2016) Multiplexing slanted spiral microchannels for ultra-fast blood plasma separation. *Lab Chip* 16(15):2791–2802
- Dincau BM, Aghilinejad A, Hammersley T, Chen X, Kim J-H (2018) Deterministic lateral displacement (DLD) in the high Reynolds number regime: high-throughput and dynamic separation characteristics. *Microfluid Nanofluid* 22(6):59
- Holm SH, Beech JP, Barrett MP, Tegenfeldt JO (2011) Separation of parasites from human blood using deterministic lateral displacement. *Lab Chip* 11(7):1326–1332

13. Huang LR, Cox EC, Austin RH, Sturm JC (2004) Continuous particle separation through deterministic lateral displacement. *Science* 304(5673):987–990
14. Loutherbak K, D'Silva J, Liu L, Wu A, Austin RH, Sturm JC (2012) Deterministic separation of cancer cells from blood at 10 mL/min. *AIP Adv* 2(4):042107
15. Jain A, Posner JD (2008) Particle dispersion and separation resolution of pinched flow fractionation. *Anal Chem* 80(5):1641–1648
16. Vig AL, Kristensen A (2008) Separation enhancement in pinched flow fractionation. *Appl Phys Lett* 93(20):203507
17. Yamada M, Nakashima M, Seki M (2004) Pinched flow fractionation: continuous size separation of particles utilizing a laminar flow profile in a pinched microchannel. *Anal Chem* 76(18):5465–5471
18. Pethig R (2010) Dielectrophoresis: status of the theory, technology, and applications. *Biomicrofluidics* 4(2):022811
19. Shafiee H, Caldwell JL, Sano MB, Davalos RV (2009) Contactless dielectrophoresis: a new technique for cell manipulation. *Biomed Microdev* 11(5):997
20. Zhu H, Lin X, Su Y, Dong H, Wu J (2015) Bioelectronics. Screen-printed microfluidic dielectrophoresis chip for cell separation. *Biosens Bioelectron* 63:371–378
21. Das D, Biswas K, Das S (2014) Physics. A microfluidic device for continuous manipulation of biological cells using dielectrophoresis. *Med Eng Phys* 36(6):726–731
22. Vykoukal J, Vykoukal DM, Freyberg S, Alt EU, Gascoyne PR (2008) Enrichment of putative stem cells from adipose tissue using dielectrophoretic field-flow fractionation. *Lab Chip* 8(8):1386–1393
23. Yunus NAM, Nili H, Green NG (2013) Continuous separation of colloidal particles using dielectrophoresis. *Electrophoresis* 34(7):969–978
24. Ding X, Li P, Lin S-CS, Stratton ZS, Nama N, Guo F, Slotcavage D, Mao X, Shi J, Costanzo F (2013) Surface acoustic wave microfluidics. *Lab Chip* 13(18):3626–3649
25. Petersson F, Åberg L, Swärd-Nilsson A-M, Laurell T (2007) Free flow acoustophoresis: microfluidic-based mode of particle and cell separation. *Anal Chem* 79(14):5117–5123
26. Shi J, Huang H, Stratton Z, Huang Y, Huang T (2009) Continuous particle separation in a microfluidic channel via standing surface acoustic waves (SSAW). *Lab Chip* 9(23):3354–3359
27. Chen Y, Wu M, Ren L, Liu J, Whitley PH, Wang L, Huang TJ (2016) High-throughput acoustic separation of platelets from whole blood. *Lab Chip* 16(18):3466–3472
28. Han K-H, Bruno Frazier A (2004) Continuous magnetophoretic separation of blood cells in microdevice format. *J Appl Phys* 96(10):5797–5802
29. Pamme N, Manz A (2004) On-chip free-flow magnetophoresis: continuous flow separation of magnetic particles and agglomerates. *Anal Chem* 76(24):7250–7256
30. Han K-H, Frazier AB (2005) Diamagnetic capture mode magnetophoretic microseparator for blood cells. *J Microelectromech Syst* 14(6):1422–1431
31. Han K-H, Frazier AB (2005) A microfluidic system for continuous magnetophoretic separation of suspended cells using their native magnetic properties. *Proc Nanotechol* 1:187–190
32. Tzirtzilakis E (2005) A mathematical model for blood flow in magnetic field. *Phys Fluids* 17(7):077103
33. Furlani EP (2007) Magnetophoretic separation of blood cells at the microscale. *J Phys D Appl Phys* 40(5):1313
34. Adams JD, Kim U, Soh HT (2008) Multitarget magnetic activated cell sorter. *Proc Natl Acad Sci* 105(47):18165–18170
35. Gijls MA, Lacharme F, Lehmann U (2010) Microfluidic applications of magnetic particles for biological analysis and catalysis. *Chem Rev* 110(3):1518–1563
36. Seo H-K, Kim H-O, Kim Y-J (2010) Hydrodynamics and magnetophoresis based hybrid blood cell sorter. In: 10th IEEE international conference on nanotechnology. IEEE, pp 911–914
37. Seo H-K, Kim Y-H, Kim H-O, Kim Y-J (2010) Hybrid cell sorters for on-chip cell separation by hydrodynamics and magnetophoresis. *J Micromech Microeng* 20(9):095019
38. Zhu T, Marrero F, Mao L (2010) Continuous separation of non-magnetic particles inside ferrofluids. *Microfluid Nanofluid* 9(4–5):1003–1009
39. Baek MK, Choi HS, Lee KS, Park IH (2011) Numerical analysis for magnetophoretic separation of blood cells in fluid and magnetic field. *IEEE Trans Appl Supercond* 22(3):4401604
40. Forbes TP, Forry SP (2012) Microfluidic magnetophoretic separations of immunomagnetically labeled rare mammalian cells. *Lab Chip* 12(8):1471–1479
41. Mizuno M, Yamada M, Mitamura R, Ike K, Toyama K, Seki M (2013) Magnetophoresis-integrated hydrodynamic filtration system for size-and surface marker-based two-dimensional cell sorting. *Anal Chem* 85(16):7666–7673
42. Nam J, Huang H, Lim H, Lim C, Shin S (2013) Magnetic separation of malaria-infected red blood cells in various developmental stages. *Anal Chem* 85(15):7316–7323
43. Zhu T, Cheng R, Liu Y, He J, Mao L (2014) Combining positive and negative magnetophoreses to separate particles of different magnetic properties. *Microfluid Nanofluid* 17(6):973–982
44. Fateen S-EK, Magdy M (2015) Design. Three dimensional simulation of negative-magnetophoretic filtration of non-magnetic nanoparticles. *Chem Eng Res Des* 95:69–78
45. Hejazian M, Li W, Nguyen N-T (2015) Lab on a chip for continuous-flow magnetic cell separation. *Lab Chip* 15(4):959–970
46. Zhou Y, Kumar DT, Lu X, Kale A, DuBose J, Song Y, Wang J, Li D, Xuan X (2015) Simultaneous diamagnetic and magnetic particle trapping in ferrofluid microflows via a single permanent magnet. *Biomicrofluidics* 9(4):044102
47. Hejazian M, Nguyen N-T (2016) Magnetofluidic concentration and separation of non-magnetic particles using two magnet arrays. *Biomicrofluidics* 10(4):044103
48. Kim MJ, Lee DJ, Youn JR, Song YS (2016) Two step label free particle separation in a microfluidic system using elasto-inertial focusing and magnetophoresis. *RSC Adv* 6(38):32090–32097
49. Zhang J, Yan S, Yuan D, Zhao Q, Tan SH, Nguyen N-T, Li W (2016) A novel viscoelastic-based ferrofluid for continuous sheathless microfluidic separation of nonmagnetic microparticles. *Lab Chip* 16(20):3947–3956
50. Zhou Y, Xuan X (2016) Diamagnetic particle separation by shape in ferrofluids. *Appl Phys Lett* 109(10):102405
51. Chen Q, Li D, Lin J, Wang M, Xuan X (2017) Simultaneous separation and washing of nonmagnetic particles in an

- inertial ferrofluid/water coflow. *Anal Chem* 89(12):6915–6920
52. Tarn MD, Pamme N (2017) On-chip magnetic particle-based immunoassays using multilaminar flow for clinical diagnostics. *Microchip diagnostics*. Springer, New York, pp 69–83
 53. Zhao W, Cheng R, Jenkins BD, Zhu T, Okonkwo NE, Jones CE, Davis MB, Kavuri SK, Hao Z, Schroeder C (2017) Label-free ferrohydrodynamic cell separation of circulating tumor cells. *Lab Chip* 17(18):3097–3111
 54. Zhao W, Cheng R, Lim SH, Miller JR, Zhang W, Tang W, Xie J, Mao L (2017) Biocompatible and label-free separation of cancer cells from cell culture lines from white blood cells in ferrofluids. *Lab Chip* 17(13):2243–2255
 55. Alnaimat F, Dagher S, Mathew B, Hilal-Alnqbi A, Khashan S (2018) Microfluidics based magnetophoresis: a review. *Chem Rec* 18(11):1596–1612
 56. Cardoso VF, Miranda D, Botelho G, Minas G, Lancers-Méndez S (2018) Highly effective clean-up of magnetic nanoparticles using microfluidic technology. *Sens. Chem. Actuat. B* 255:2384–2391
 57. Munaz A, Shiddiky MJ, Nguyen N-T (2018) Recent advances and current challenges in magnetophoresis based micro magnetofluidics. *Biomicrofluidics* 12(3):031501
 58. Munaz A, Shiddiky MJ, Nguyen N-T (2018) Chemical AB. Magnetophoretic separation of diamagnetic particles through parallel ferrofluid streams. *Sens Chem Actuat B* 275:459–469
 59. Oh S, Jung SH, Seo H, Min M-K, Kim B, Hahn YK, Kang JH, Choi S (2018) Magnetic activated cell sorting (MACS) pipette tip for immunomagnetic bacteria separation. *Sens Chem Actuat B* 272:324–330
 60. Wu J, Cui Y, Xuan S, Gong X (2018) Nanofluidics. 3D-printed microfluidic manipulation device integrated with magnetic array. *Microfluidics and Nanofluidics* 22(9):103
 61. Lin S, Zhi X, Chen D, Xia F, Shen Y, Niu J, Huang S, Song J, Miao J, Cui D (2019) A flyover style microfluidic chip for highly purified magnetic cell separation. *Biosens Bioelectron* 129:175–181
 62. Watarai H, Namba M (2002) Capillary magnetophoresis of human blood cells and their magnetophoretic trapping in a flow system. *J Chromatogr A* 961(1):3–8
 63. Zborowski M, Ostera GR, Moore LR, Milliron S, Chalmers JJ, Schechter AN (2003) Red blood cell magnetophoresis. *Biophys J* 84(4):2638–2645
 64. Vanderlinde J (2006) Classical electromagnetic theory. Springer, New York, p 145
 65. Cheng R, Zhu T, Mao L (2014) Three-dimensional and analytical modeling of microfluidic particle transport in magnetic fluids. *Microfluid Nanofluid* 16(6):1143–1154
 66. He Y, Luo L, Huang S (2019) Magnetic manipulation on the unlabeled nonmagnetic particles. *Int J Mod Phys B* 33(07):1950047
 67. Bayareh M, Nazemi Ashani M, Usefian A (2020) Active and passive micromixers: a comprehensive review. *Chem Eng Process Process Intensif* 147:107771. <https://doi.org/10.1016/j.cep.2019.107771>

Publisher's Note Springer Nature remains neutral with regard to jurisdictional claims in published maps and institutional affiliations.